DOI: http://dx.doi.org/10.32571/ijct.1060520 E-ISSN: 2602-277X

International Journal of Chemistry and Technology

http://dergipark.org.tr/ijct

Research Article

Heat energy transport characteristics of microchannel reactors for hydrogen production by steam-methanol reforming on copper-based catalysts

Junjie CHEN[1,*]

[1] *Department of Energy and Power Engineering, School of Mechanical and Power Engineering, Henan Polytechnic University, 2000 Century Avenue, Jiaozuo, Henan, 454000, P.R. China*

Received: 20 April January 2022; Revised: 3 November 2022; Accepted: 8 November 2022

*Corresponding author e-mail: cjjtpj@163.com

Citation: Chen, J. *Int. J. Chem. Technol.* **2023**, 7 (1), 57-66.

ABSTRACT

Numerical simulations are carried out to understand the heat energy transport characteristics of microchannel reactors for hydrogen production by steam-methanol reforming on copper-based catalysts. Enthalpy analysis is performed and the evolution of energy in the oxidation and reforming processes is discussed in terms of reaction heat flux. The effects of solid thermal conductivity, gas velocity, and flow arrangement on the thermal behavior of the reactor is evaluated in order to fully describe the thermal energy change in the reactor. The results indicate that the thermal behavior of the reactor depends upon the thermal properties of the walls. The change in enthalpy is of particular importance in exothermic and endothermic reactions. The net enthalpy change for oxidation and reforming is negative and positive, but the net sensible enthalpy change is always positive in the reactor. The wall heat conduction effect accompanying temperature changes is important to the autothermal design and self-sustaining operation of the reactor. The solid thermal conductivity is of great importance in determining the operation and efficiency of the reactor. The reaction proceeds rapidly and efficiently only at high solid thermal conductivity. The reaction heat flux for oxidation and reforming is positive and negative. The change in flow arrangement significantly affects the reaction heat flux in the reactor. The parallel flow design is advantageous for purposes of enhancing heat transfer and avoiding localized hot spots.

Keywords: Hydrogen production, thermal properties, reforming reactions, oxidation reactions, flow arrangements, heat fluxes.

1. INTRODUCTION

Steam reforming reactions have vast importance in chemical reaction engineering.[1,2] Steam reforming reactions are endothermic, accompanied by the consumption of a large amount of heat.[3,4] Accordingly, heat energy transport is considered essential for steam reforming. This endothermic process involves a variety of individual reactions leading to the desired product hydrogen and undesired product carbon monoxide. The amount of heat energy must be large to make steam reforming reactions proceed rapidly in reformers containing an array of tubes.[5,6] For example, steam-methane reforming reactions proceed usually at temperatures from around 800 °C to around 900 °C.[7,8] The rate of steam-methane reforming reactions depends upon both pressure and temperature. The heat-supplying furnaces usually operate at much higher temperatures. Heating devices for hydrogen production utilize industrial flames in furnaces, and reformer design is often decided empirically, including operation conditions and reaction routes. Diffusion flames can be designed for these purposes.

Optimization of endothermic steam reforming processes in its practical hydrogen fuel cell applications can be made possible with the results of investigations about heat energy transport characteristics. Hydrocarbons and alcohols can be converted to hydrogen-rich gas, and steam reforming processes are the most primary method for hydrogen production. The need for power generation creates new opportunities for the development of hydrogen fuel cells.[9,10] Hydrogen fuel cells are important in supporting power not only for remote areas but also for inaccessible areas.[11,12] Hydrogen fuel cells are also of importance in the transportation field.[13,14] Practical hydrogen fuel cells are necessarily complex systems. Hydrogen fuel cells can convert a fuel to useful energy at a very high level of efficiency, including heptane[15,16], methane [17,18], methanol [19,20], kerosene[21], and gasoline[22],

DOI: http://dx.doi.org/10.32571/ijct.1060520 E-ISSN: 2602-277X

and therefore much less fuel is required for specify requirements of energy.

Microchannel reactors are being developed for hydrogen fuel cell purposes. Autothermal methods can be used to maintain the required temperatures with internal heating by catalytic combustion.[23] Alternating reforming and combustion spaces are designed for this purpose, but precise rates of fuel and steam or air are required for the two preceding processes with substantially lower reaction temperatures than conventional methods. Such microchannel reactors offer design and efficiency advantages,[24] depending upon factors responsible for the rate of the reforming reaction, for example, the conductive heating area.[25,26] Higher conversion can be achieved due to the improved heat energy transport characteristics, but this type of reactor has its specified temperature design range. Additionally, the loss in pressure drop is a primary concern in reactor design.

Heat integrated reactors are being developed to properly address the above concern. [27] Heat recirculation methods are employed and a concentric cylinder geometry is used, which will lead to improvements in heat energy transport. Additionally, structured catalysts are used to reduce the pressure drop across the cylindrical tubes.[27,28] Compact design methods can be used to take advantages of the large heat energy transport area of the reactor. In this case, reforming and combustion reactions can proceed simultaneously at the specified temperatures. However, scale-up issues must be addressed for this type of reactor, and the inherent advantages of this design remain to be further exploited, for example, by improving its heat energy transport characteristics.

Heat integrated reactors offer distinct advantages of carrying out simultaneous multiple chemical reactions, for example, reforming and combustion.[29,30] The heat energy released from combustion processes is used to meet the heat demand of reforming processes.[31,32] The two important influencing factor in determining the feasibility for heat recirculation are the quantity of heat produced and the temperature of the dividing walls.[33,34] These influencing factor must be controllable in the reforming process, and heat energy transport occurs through conduction across the dividing walls.[35,36] With the use of heat integrated reactors, scale-up issues and heat recirculation needs can be addressed.[37,38] Additionally, heat integrated reactors offer improvements in both heat and mass transport.[39,40] While heat exchanger methods are used extensively, the mechanism differs from that of heat integrated reactors in that multiple chemical reactions occur, for example, reforming and combustion.[41,42] Steam reforming and heat integrated reactors are of importance in hydrogen production and useful for practical applications in hydrogen fuel cells.[43,44] However, the heat energy transport characteristics of heat integrated reactors with flow microchannels are still not fully understood.

The present study relates to hydrogen production in a microchannel reactor by steam-methanol reforming on copper-based catalysts. Mathematical expressions are derived for the reactor system based upon the principles of chemical kinetics and fluid mechanics. Numerical simulations are carried out to understand the heat energy transport characteristics of the autothermal reactor. Enthalpy analysis is performed and the evolution of energy in the oxidation and reforming processes is discussed in terms of reaction heat flux. The effects of solid thermal conductivity, gas velocity, and flow arrangement on the thermal behavior of the autothermal reactor is evaluated in order to fully describe the thermal energy change in the reactor. The objective of the present study is to understand the heat energy transport characteristics of microchannel reactors for hydrogen production by steam-methanol reforming on copper-based catalysts. Emphasis is placed on the effects of solid thermal conductivity, gas velocity, and flow arrangement on the thermal behavior of autothermal reactors.

2. METHODS

2.1. Reactor representation

The complex reactor must be adaptable to continuous self-sustaining operation of the steady-stream type, and the wall material must be selected for strength. The complex reactor for producing hydrogen is illustrated schematically in Figure 1 by steam-methanol reforming on a copper-based catalyst. The reactor operates upon the principles of chemical kinetics and fluid mechanics. The channels can be designed using different flow arrangement methods.[45,46] The channels are coated with a catalyst, and the reactor walls are constructed of stainless steel.

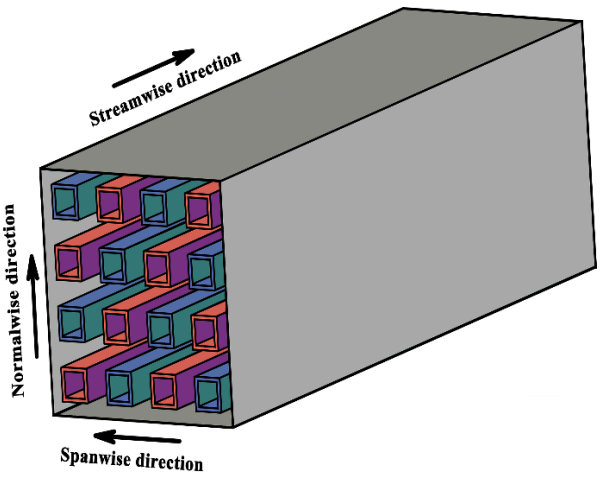

Figure 1. Schematic representation of the complex reactor for producing hydrogen by steam-methanol reforming on a copper-based catalyst.

DOI: http://dx.doi.org/10.32571/ijct.1060520 E-ISSN: 2602-277X

At the channel inlets, the pressure of the mixtures is 20 atmospheres and the temperature is 100 °C. The molar ratio of steam to carbon is 140.0:100.0 and the mole ratio of methanol to air is 11.2:100.0. At the channel inlets, the gas velocity is 0.6 and 2.0 m/s, respectively, for the oxidation and reforming reactant streams. The channels are 700 microns in height and in width, 50.0 mm in length, and square in cross section. The solid thermal conductivity is 200 W/(m·K) at a temperature of 20 °C. The structured catalyst is 100 microns in thickness. The un-coated walls are 700 microns in thickness.

The computational domain of the complex reactor for producing hydrogen is illustrated schematically in Figure 2 by steam-methanol reforming. The energy released in the oxidation process is the basis of the complex reactor. The oxidation and reforming reactions must be sustained at constant rates and maintained at a controlled level.[47,48] In this case, the operation of the reactor will remain steady. The oxidation and reforming reactions must proceed at temperatures above 200 °C but below 300 °C. During reactor start-up, the gas mixtures are ignited in the oxidation channels. Properly ignited, the energy released in the oxidation process must raise the temperature of the reactor sufficiently.

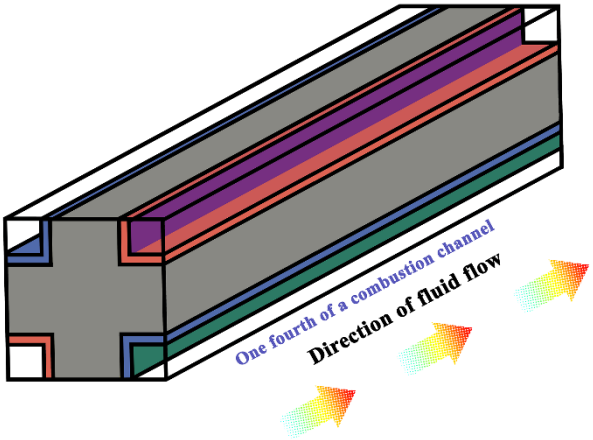

Figure 2. Schematic representation of the computational domain of the complex reactor for producing hydrogen by steam-methanol reforming.

2.2. Mathematical representation

The structured mesh of the complex reactor for producing hydrogen is illustrated in Figure 3 by steam-methanol reforming on a copper-based catalyst. Oxidation and reforming in the reactor are complex physical and chemical process processes. Under the reaction conditions specified above, mathematical expressions are derived for the reactor system.

The mechanism of the oxidation or reforming reaction can be represented as

$$\sum_{s=1}^{K_s} \nu'_{si}\chi_s \Leftrightarrow \sum_{s=1}^{K_s} \nu''_{si}\chi_s\,, (i = 1, \dots, \delta) \quad (1)$$

where K_s is the number of species, ν is the stoichiometric coefficient, χ_s is the surface species s, and δ is the number of surface reactions.

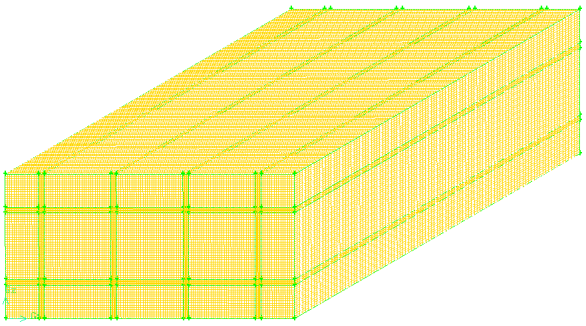

Figure 3. Structured mesh of the complex reactor for producing hydrogen by steam-methanol reforming on a copper-based catalyst.

The production rate $\dot{s}_s$ is given by

$$\dot{s}_s = \sum_{i=1}^{I} \nu_{si} q_i\,, (s = 1, \dots, K_s), \quad (2)$$

$$\nu_{si} = \nu''_{si} - \nu'_{si}. \quad (3)$$

The rate-of-progress variable q_i is defined as

$$q_i = k_{fi} \prod_{s=1}^{K_s} [\chi_s]^{\nu'_{si}} - k_{ri} \prod_{s=1}^{K_s} [\chi_s]^{\nu''_{si}}, \quad (4)$$

where k is the rate constant.

The forward reaction rate constant is defined as

$$k_{fi} = A_i T^{\beta_i} e^{\frac{-E_i}{RT}}, \quad (5)$$

where β is the temperature exponent, E is the activation energy, and A is the pre-exponential factor.

The reverse reaction rate constant is defined as

$$k_{ri} = \frac{k_{fi}}{K_{ci}}, \quad (6)$$

where K is the equilibrium constant.

The gas-phase species must be balanced in each channel:

$$\frac{\partial}{\partial x}(\rho w_k V_{k,x}) + \frac{\partial}{\partial y}(\rho w_k V_{k,y}) + \frac{\partial}{\partial z}(\rho w_k V_{k,z}) + \frac{\partial(\rho u_x w_k)}{\partial x} + \frac{\partial(\rho u_y w_k)}{\partial y} + \frac{\partial(\rho u_z w_k)}{\partial z} - \dot{\xi}_k W_k = 0, \quad (7)$$

where x, y, and z are coordinate variables, k denotes gas-phase species, V is the diffusion velocity, W is the molecular mass, ρ is the density, w is the mass fraction, and $\dot{\xi}$ is the gas-phase reaction rate.

The Knudsen diffusivity is calculated in terms of mean pore diameter d as

DOI: http://dx.doi.org/10.32571/ijct.1060520 E-ISSN: 2602-277X

$$D_i^K = \frac{d}{3}(8RT)^{\frac{1}{2}}(\pi W_i)^{-\frac{1}{2}}. \quad (8)$$

The momentum balance in each channel can be stated as

$$\frac{\partial}{\partial x}\left[\mu\left(\frac{\partial u_x}{\partial x}+\frac{\partial u_x}{\partial x}\right)\right]+\frac{\partial}{\partial y}\left[\mu\left(\frac{\partial u_x}{\partial y}+\frac{\partial u_y}{\partial x}\right)\right]+\frac{\partial}{\partial z}\left[\mu\left(\frac{\partial u_x}{\partial z}+\frac{\partial u_z}{\partial x}\right)\right]-\frac{\partial}{\partial x}\left[\frac{2}{3}\mu\left(\frac{\partial u_{xx}}{\partial x}+\frac{\partial u_{yx}}{\partial y}+\frac{\partial u_{zx}}{\partial z}\right)\right]-\frac{\partial p}{\partial x}=0, \quad (9)$$

$$\frac{\partial}{\partial x}\left[\mu\left(\frac{\partial u_y}{\partial x}+\frac{\partial u_x}{\partial y}\right)\right]+\frac{\partial}{\partial y}\left[\mu\left(\frac{\partial u_y}{\partial y}+\frac{\partial u_y}{\partial y}\right)\right]+\frac{\partial}{\partial z}\left[\mu\left(\frac{\partial u_y}{\partial z}+\frac{\partial u_z}{\partial y}\right)\right]-\frac{\partial}{\partial y}\left[\frac{2}{3}\mu\left(\frac{\partial u_{xy}}{\partial x}+\frac{\partial u_{yy}}{\partial y}+\frac{\partial u_{zy}}{\partial z}\right)\right]-\frac{\partial p}{\partial y}=0, \quad (10)$$

$$\frac{\partial}{\partial x}\left[\mu\left(\frac{\partial u_z}{\partial x}+\frac{\partial u_x}{\partial z}\right)\right]+\frac{\partial}{\partial y}\left[\mu\left(\frac{\partial u_z}{\partial y}+\frac{\partial u_y}{\partial z}\right)\right]+\frac{\partial}{\partial z}\left[\mu\left(\frac{\partial u_z}{\partial z}+\frac{\partial u_z}{\partial z}\right)\right]-\frac{\partial}{\partial z}\left[\frac{2}{3}\mu\left(\frac{\partial u_{xz}}{\partial x}+\frac{\partial u_{yz}}{\partial y}+\frac{\partial u_{zz}}{\partial z}\right)\right]-\frac{\partial p}{\partial z}=0, \quad (11)$$

where μ is the dynamic viscosity, u is the velocity, and p is the pressure.

The mass must also be balanced in each channel:

$$\frac{\partial(\rho u_x)}{\partial x}+\frac{\partial(\rho u_y)}{\partial y}+\frac{\partial(\rho u_z)}{\partial z}=0. \quad (12)$$

The conservation of energy in each channel can be stated as

$$\frac{\partial}{\partial x}\left(-k_g\frac{\partial T}{\partial x}+\rho\sum_{k=1}^{\gamma}w_k h_k V_{k,x}\right)+\frac{\partial}{\partial y}\left(-k_g\frac{\partial T}{\partial y}+\rho\sum_{k=1}^{\gamma}w_k h_k V_{k,y}\right)+\frac{\partial}{\partial z}\left(-k_g\frac{\partial T}{\partial z}+\rho\sum_{k=1}^{\gamma}w_k h_k V_{k,z}\right)+\frac{\partial(\rho u_x h)}{\partial x}+\frac{\partial(\rho u_y h)}{\partial y}+\frac{\partial(\rho u_z h)}{\partial z}=0, \quad (13)$$

where γ is the number of gas-phase species, k is the thermal conductivity, g denotes the gas mixture, T is the temperature, and h is the enthalpy.

The chemical species must be balanced on each catalyst surface:

$$\frac{\theta_m\dot{\zeta}_m}{\gamma'}=0, \quad (14)$$

where θ is the coverage, m denotes surface species, γ' is the site density, and $\dot{\zeta}$ is the reaction rate.

The conservation of energy in each wall can be stated as

$$\frac{\partial}{\partial x}\left(k_{wall}\frac{\partial T}{\partial x}\right)+\frac{\partial}{\partial y}\left(k_{wall}\frac{\partial T}{\partial y}\right)+\frac{\partial}{\partial z}\left(k_{wall}\frac{\partial T}{\partial z}\right)=0. \quad (15)$$

2.3. Chemistry representation

The oxidation reaction is described by

$$CH_3OH + 1.5O_2 \Leftrightarrow 2H_2O + CO_2. \quad (16)$$

The reforming reactions are described by

$$CH_3OH + H_2O \Leftrightarrow 3H_2 + CO_2. \quad (17)$$

$$CH_3OH \Leftrightarrow 2H_2 + CO. \quad (18)$$

The water-gas shift reaction is described by

$$CO + H_2O \Leftrightarrow H_2 + CO_2. \quad (19)$$

The oxidation and reforming processes are accounted for by chemical kinetic models.[49,50] The reforming reaction rate is given by

$$r_{reforming}=\left[k_R K^{\vartheta}_{CH_3O^{(\alpha)}}\left(p_{CH_3OH}p_{H_2}^{-0.5}\right)\left(1-k_R^{-1}p_{H_2}^3 p_{CO_2}p_{CH_3OH}^{-1}p_{H_2O}^{-1}\right)c_{S_\alpha}^{\pi}c_{S_{\alpha a}}^{\pi}\right]\cdot\left[\left(1+K^{\vartheta}_{CH_3O^{(\alpha)}}\left(p_{CH_3OH}p_{H_2}^{-0.5}\right)+K^{\vartheta}_{HCOO^{(\alpha)}}p_{CO_2}p_{H_2}^{0.5}+K^{\vartheta}_{OH^{(\alpha)}}\left(p_{H_2O}p_{H_2}^{-0.5}\right)\right)\left(1+K_{H^{(\alpha a)}}^{0.5}p_{H_2}^{0.5}\right)\right]^{-1}, \quad (20)$$

where c^{π} is the total surface concentration and ϑ denotes the composite parameter.

The water-gas shift reaction rate is given by

$$r_{water-gas\ shift}=\left[k_W^{\vartheta}K^{\vartheta}_{OH^{(\alpha)}}\left(p_{CO}p_{H_2O}p_{H_2}^{-0.5}\right)\left(1-k_W^{-1}p_{H_2}p_{CO_2}p_{CO}^{-1}p_{H_2O}^{-1}\right)\left(c_{S_\alpha}^{\pi}\right)^2\right]\cdot\left[\left(1+K^{\vartheta}_{CH_3O^{(\alpha)}}\left(p_{CH_3OH}p_{H_2}^{-0.5}\right)+K^{\vartheta}_{HCOO^{(\alpha)}}p_{CO_2}p_{H_2}^{0.5}+K^{\vartheta}_{OH^{(\alpha)}}\left(p_{H_2O}p_{H_2}^{-0.5}\right)\right)\right]^{-2}. \quad (21)$$

The decomposition reaction rate is given by

$$r_{decomposition}=\left[k_D K^{\vartheta}_{CH_3O^{(\beta)}}\left(p_{CH_3OH}p_{H_2}^{-0.5}\right)\left(1-k_D^{-1}p_{H_2}^2 p_{CO}p_{CH_3OH}^{-1}\right)c_{S_\beta}^{\pi}c_{S_{\beta a}}^{\pi}\right]\cdot\left[\left(1+K^{\vartheta}_{CH_3O^{(\beta)}}\left(p_{CH_3OH}p_{H_2}^{-0.5}\right)+K^{\vartheta}_{OH^{(\beta)}}\left(p_{H_2O}p_{H_2}^{-0.5}\right)\right)\left(1+K_{H^{(\beta a)}}^{0.5}p_{H_2}^{0.5}\right)\right]^{-1}. \quad (22)$$

2.4. Model validation

Comparisons are performed between the predicted results and the data obtained by measurements.[51,52] The reaction temperature remains constant. The channels are 600 microns in height, 500 microns in width, 33.0 mm in length, and rectangular in cross section. The reaction temperature is 200 °C, 220 °C, 240 °C, and 260 °C,

DOI: http://dx.doi.org/10.32571/ijct.1060520 E-ISSN: 2602-277X

respectively. The effect of reaction temperature is illustrated in Figure 4 and Figure 5 in terms of the rate of hydrogen production and the conversion of methanol. The predicted results agree with the data obtained by measurements.

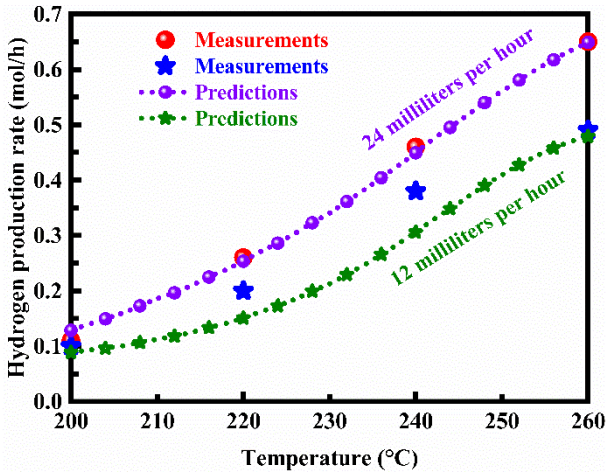

Figure 4. Effect of reaction temperature on the rate of hydrogen production. The data obtained by measurements[51,52] are also presented to validate the model.

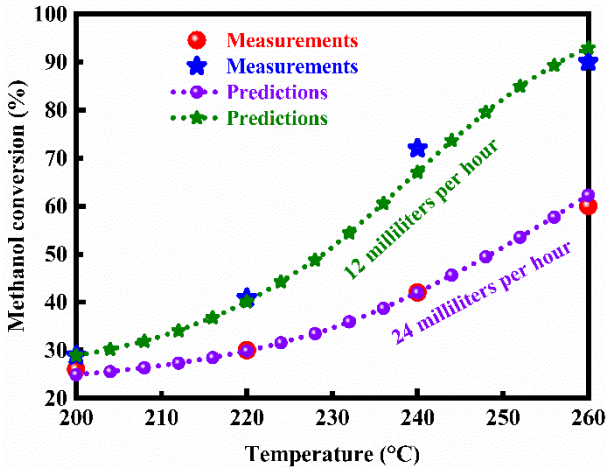

Figure 5. Effect of reaction temperature on the conversion of methanol. The data obtained by measurements[51,52] are also presented to validate the model.

3. RESULTS AND DISCUSSION

3.1. Enthalpy analysis

Enthalpy is a particularly important concept in the design of an autothermal reactor. The enthalpy contour maps in the reactor are illustrated in Figure 6 with different solid thermal conductivity. The reactor walls are constructed of stainless steel, and the behavior of fluids in the reactor can be fully described by laminar flow. Enthalpy can be entirely calculated by the local composition, pressure, and temperature in the reactor, depending upon the volume, pressure, and internal energy. The amount of heat evolved in the chemical reactions is calculated for the reactor, including the amount of heat released and absorbed. The exchange of heat arises from the difference in temperature between adjacent channels of the reactor. Various efficient heat exchange methods offer the opportunity to design microchannel reactors.[53,54] Both dimensions and geometry are very important from the standpoint of design.[55,56] The heat released by the oxidation reaction accounts for the temperature rise in the reactor. The heat energy released by the oxidation reaction is much greater than the heat energy consumed by the reforming reaction. However, the total energy contained in the reactor is conserved. The oxidation and reforming reactions occur rapidly in the reactor. However, oxidation differs from reforming in enthalpy change, depending upon the solid thermal conductivity. The change in enthalpy is of particular importance in exothermic and endothermic reactions, as heat must be balanced in the reactor. The net enthalpy change for oxidation is negative at constant pressure, as an amount of energy flows out of its channels. The net enthalpy change is positive for reforming at constant pressure, as an amount of energy flows into its channels. While the oxidation and reforming reactions proceed in the reactor, the total amount of energy does not change. The thermal behavior of the reactor depends upon the thermal properties of the walls. The net enthalpy change is thermal conductivity-dependent. The concept of thermal conductivity is fundamental to the design of the autothermal reactor. The importance of thermal conductivity will be discussed in more detail below. The net enthalpy change at low thermal conductivity is small for either oxidation or reforming. In contrast, the net enthalpy change is significant at high thermal conductivity.

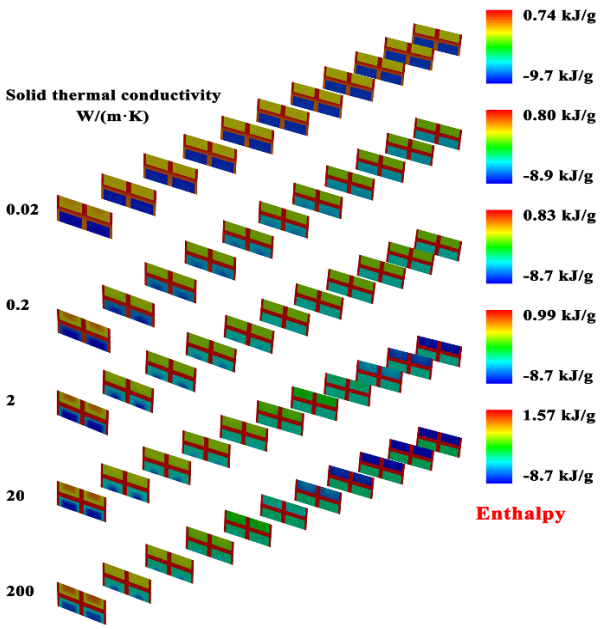

Figure 6. Enthalpy contour maps in the reactor with different solid thermal conductivity. The reactor walls are constructed of stainless steel.

DOI: http://dx.doi.org/10.32571/ijct.1060520 E-ISSN: 2602-277X

The sensible enthalpy change is accompanied by the change in temperature. The sensible enthalpy contour maps in the reactor are illustrated in Figure 7 with different solid thermal conductivity. The net change between the sensible enthalpy at the end of the oxidation or reforming reaction and the sensible enthalpy at the start of the reaction is always positive in the reactor. The net sensible enthalpy change accompanying the reforming process is small at low thermal conductivity. The net sensible enthalpy change accompanying the oxidation process is large at high thermal conductivity. In contrast, the net sensible enthalpy change is significant for reforming at high thermal conductivity or for oxidation at low thermal conductivity. Furthermore, the net sensible enthalpy change depends upon not only the solid thermal conductivity but also the chemical reaction. Consequently, the net sensible enthalpy change is always positive in the reactor, but depending upon the solid thermal conductivity and the chemical reaction. Due to the overall increase in sensible enthalpy, the reforming reaction is product-favored.

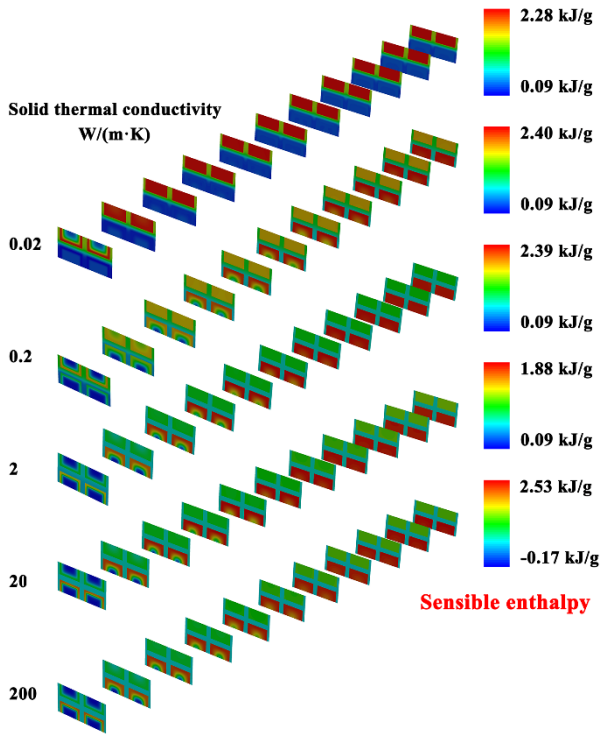

Figure 7. Sensible enthalpy contour maps in the reactor with different solid thermal conductivity. The reactor walls are constructed of stainless steel.

The species mole fraction contour maps in the reactor are illustrated in Figure 8 when the reactor walls are constructed of stainless steel. The reforming reaction proceeds rapidly in the reactor and the conversion is nearly complete due to the high solid thermal conductivity. Energy is evolved in the reactor in the form of heat as the oxidation and reforming reactions proceed simultaneously. The production of hydrogen from methanol is always endothermic. The amount of carbon monoxide is very small doe to almost complete conversion of methanol to carbon dioxide, which is of great importance in practical hydrogen fuel cell applications. The endothermic reaction occurs rapidly since stainless steel is better at conducting heat between adjacent channels of the reactor.

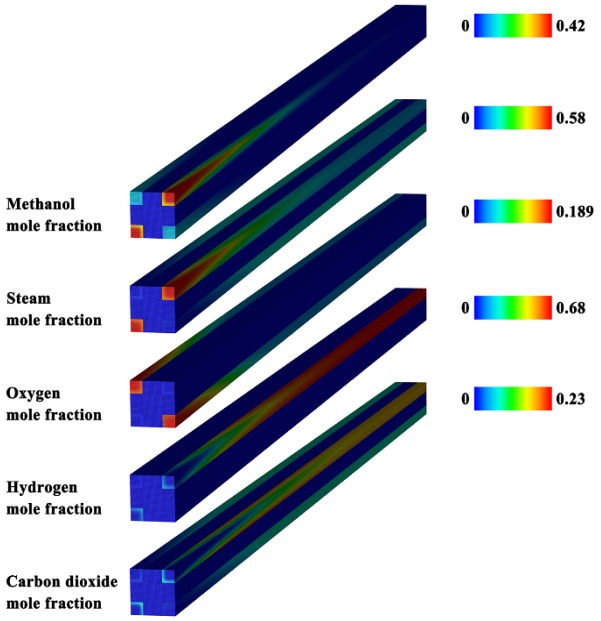

Figure 8. Species mole fraction contour maps in the microchannel reactor when the reactor walls are constructed of stainless steel.

3.2. Effect of solid thermal conductivity

The effect of solid thermal conductivity is studied in order to fully describe the thermal energy change in the reactor. The temperature contour maps in the microchannel reactor are illustrated in Figure 9 with different solid thermal conductivity. The solid thermal conductivity is 0.02, 0.2, 2, 20, and 200 W/(m·K), respectively. The reactor walls are constructed of stainless steel. The temperature in the reactor is thermal conductivity-dependent. The heat effect accompanying the change in solid thermal conductivity is manifested by decreases or increases in reactor temperature. Appropriate values of solid thermal conductivity are necessary for the design of the autothermal microchannel reactor for use in the steam-methanol reforming process. Since heat does flow from the oxidation region to the reforming region, the reactor temperature depends up not only the solid thermal conductivity but also the amount of heat evolved in the oxidation and reforming processes. The reforming region absorbs heat with an increase in temperature, and the oxidation region generates heat with also an increase in temperature. An exact relationship exists between the amounts of heat absorbed and generated and the amount of heat required to raise the temperatures of both the oxidation and reforming regions. The wall heat conduction effect accompanying

DOI: http://dx.doi.org/10.32571/ijct.1060520 E-ISSN: 2602-277X

temperature changes is important to the autothermal design and self-sustaining operation of the reactor. The total energy of the reactor system is constant. The amount of heat involved in the processes can be calculated at constant pressure based on the principles of thermodynamics, since the amount of heat involved in the oxidation and reforming processes depends partly upon pressure. All the heat flowing into the reforming channels raises the temperature of the gas mixture so that the reactants can be converted to the desired product hydrogen. At low solid thermal conductivity, the difference in temperature between the oxidation and reforming regions is very large, which leads to steep temperature gradients. At high solid thermal conductivity, the difference in temperature between the oxidation and reforming regions is very small, accompanied by very small temperature gradients. The solid thermal conductivity is of great importance in determining the operation and efficiency of the reactor. The reaction proceeds rapidly and efficiently only at high solid thermal conductivity. In this case, the solid thermal conductivity greatly contributes to transport of energy between the oxidation and reforming regions. Conditions must be such that the walls are highly conductive solids.

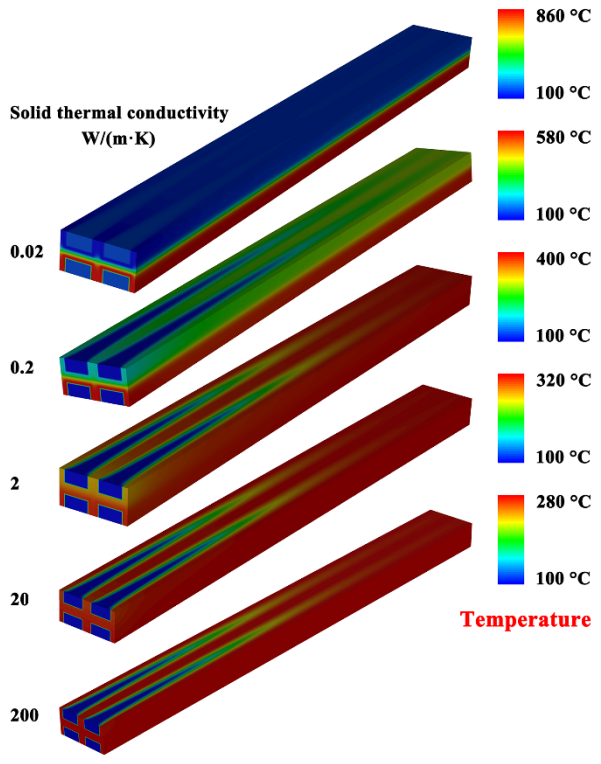

Figure 9. Temperature contour maps in the microchannel reactor with different solid thermal conductivity. The reactor walls are constructed of stainless steel.

The effect of solid thermal conductivity on the hydrogen yield of the microchannel reactor is illustrated in Figure 10 at different inlet gas velocities. The solid thermal conductivity is 0. 2, 0.6, 2, 6, 20, and 60 W/(m·K), respectively. At the channel inlets, the gas velocity is 0.6 and 2.0 m/s or 0.6 and 3.0 m/s for the oxidation and reforming reactant streams. The hydrogen yield generally increases with solid thermal conductivity, and the reactions must therefore be carried out in the reactor with high solid thermal conductivity, at which methanol reacts so rapidly steam that the conversion is nearly complete. At high flow rates for the reforming reactant stream, the conversion is incomplete due to the excess absorption of thermal energy in the reforming region, since heat must be balanced in the reactor. Accordingly, the hydrogen yield is relatively low, especially at low solid thermal conductivity. Stainless steel is cost effective and has relatively high thermal conductivity. When the reactor walls are constructed of stainless steel, nearly complete conversion can be achieved in the reactor.

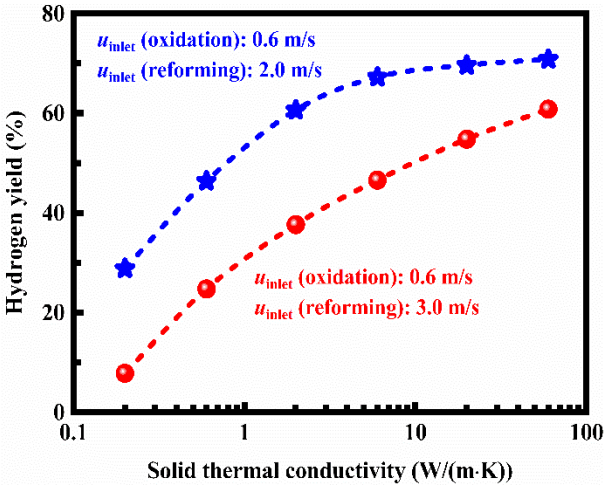

Figure 10. Effect of solid thermal conductivity on the hydrogen yield of the microchannel reactor at different inlet gas velocities.

3.3. Reaction heat fluxes

The effect of gas velocity on the thermal behavior of the reactor is evaluated based upon reaction heat flux in order to understand the evolution of heat in the system. The effect of the gas velocity at the channel inlets on the heat fluxes of the oxidation and reforming reactions is illustrated in Figure 11 for the reactor. The reaction heat flux for oxidation and reforming is positive and negative, respectively. The reaction heat flux for oxidation is positive, since the heat released by the oxidation reaction flows out of its region.

The reaction heat flux for reforming is negative, since the heat consumed by the reforming reaction flows into its region. The reaction heat flux in magnitude increases with the gas velocity when heat is balanced in the reactor. The positive heat flux is larger in magnitude than the negative heat flux, and therefore the net reaction heat flux is positive. There is a mathematical relation between heat flux and temperature gradient, depending upon the solid thermal conductivity. The total heat flux across the walls

DOI: http://dx.doi.org/10.32571/ijct.1060520 E-ISSN: 2602-277X

is proportional to the gradient of temperature within the walls.

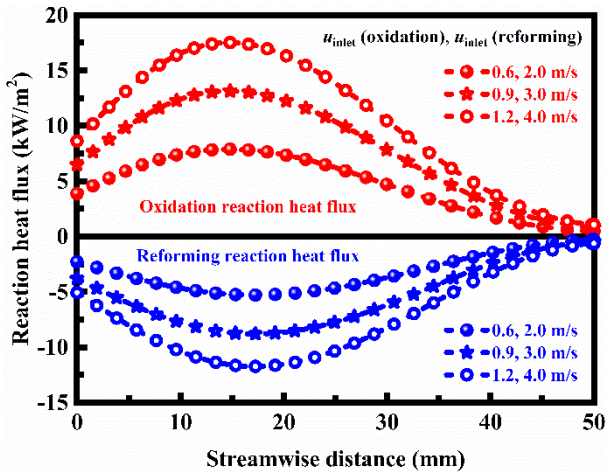

Figure 11. Effect of the gas velocity at the channel inlets on the heat fluxes of the oxidation and reforming reactions in the reactor.

The effect of flow arrangement on the heat fluxes of the oxidation and reforming reactions is illustrated in Figure 12 for the reactor. The heat flux results are presented for the parallel flow design and for the counter-current design. Several factors influence the operation of an autothermal reactor.[57,58] The factor considered here is the flow arrangement.

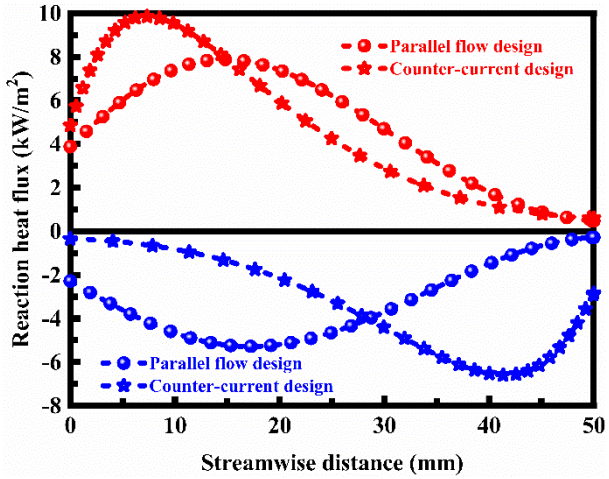

Figure 12. Effect of flow arrangement on the heat fluxes of the oxidation and reforming reactions in the reactor. The heat flux results are presented for the parallel flow design and for the counter-current design.

4. CONCLUSIONS

Numerical simulations are carried out to understand the thermal transport characteristics of autothermal reactors for hydrogen production. Enthalpy analysis is performed and the evolution of energy in the chemical processes is discussed based upon heat flux. The effects of solid thermal conductivity, gas velocity, and flow arrangement on the thermal behavior of the reactor is evaluated in order to fully describe the thermal energy change in the reactor. The major conclusions are summarized as follows:

- Oxidation differs from reforming in enthalpy change, depending upon the solid thermal conductivity. The change in enthalpy is of particular importance in exothermic and endothermic reactions.
- The net enthalpy change for oxidation and reforming is negative and positive, respectively. The thermal behavior of the reactor depends upon the thermal properties of the walls. The net enthalpy change is thermal conductivity-dependent.
- The net sensible enthalpy change is always positive in the reactor, but depending upon the solid thermal conductivity and the chemical reaction.
- The reactor temperature is also thermal conductivity-dependent. The wall heat conduction effect accompanying temperature changes is important to the autothermal design and self-sustaining operation of the reactor.
- The solid thermal conductivity is of great importance in determining the operation and efficiency of the reactor. The reaction proceeds rapidly and efficiently only at high solid thermal conductivity.
- The reaction heat flux for oxidation and reforming is positive and negative, respectively. The positive heat flux is larger in magnitude than the negative heat flux, and the net reaction heat flux is positive.
- The change in flow arrangement significantly affects the reaction heat flux in the reactor. The parallel flow design is advantageous for purposes of enhancing heat transfer and avoiding localized hot spots.

Conflict of interests

I declares that there is no a conflict of interest with any person, institute, company, etc.

REFERENCES

1. Ming, Q.; Healey, T.; Allen, L.; Irving, P. *Catal. Today* 77(1-2), 2002, 51-64.

2. Rostrup-Nielsen, J.R. *Catal. Today* 145(1-2), 2009, 72-75.

3. Dincer, I. *Int. J. Hydrogen Energy* 37(2), 2012, 1954-1971.

DOI: http://dx.doi.org/10.32571/ijct.1060520 E-ISSN: 2602-277X

4. Muradov N.Z.; Veziroğlu, T.N. *Int. J. Hydrogen Energy* 30(3), 2005, 225-237.

5. Tacchino, V.; Costamagna, P.; Rosellini, S.; Mantelli, V.; Servida, A. *Chem. Eng. J.* 428, 2022, 131492.

6. Tutar, M.; Üstün, C.E.; Campillo-Robles, J.M.; Fuente, R.; Cibrián, S.; Arzua, I.; Fernández, A.; López, G.A. *Comput. Chem. Eng.* 155, 2021, 107504.

7. Wang, J.; Wei, S.; Wang, Q.; Sundén, B. *Int. J. Hydrogen Energy* 46(29), 2021, 15241-15256.

8. Taji, M.; Farsi, M.; Keshavarz, P. *Int. J. Hydrogen Energy* 43(29), 2018, 13110-13121.

9. Fadzillah, D.M.; Kamarudin, S.K.; Zainoodin, M.A.; Masdar, M.S. *Int. J. Hydrogen Energy* 44(5), 2019, 3031-3054.

10. Wang, Y.; Diaz, D.F.R.; Chen, K.S.; Wang, Z.; Adroher, X.C. *Mater. Today* 32, 2020, 178-203.

11. Zhang, X.; Jin, Y.; Li, D.; Xiong, Y. *J. Power Sources* 506, 2021, 230135.

12. Alias, M.S.; Kamarudin, S.K.; Zainoodin, A.M.; Masdar, M.S. *Int. J. Hydrogen Energy* 45(38), 2020, 19620-19641.

13. Luo, M; Zhang, J.; Zhang, C.; Chin, C.S.; Ran, H.; Fan, M.; Du, K.; Shuai, Q. *Appl. Therm. Eng.* 201, 2022, 117816.

14. Wei, X.; Leng, J.; Sun, C.; Huo, W.; Ren, Q.; Sun, F. *J. Power Sources* 518, 2022, 230598.

15. Rakib, M.A.; Grace, J.R.; Lim, C.J.; Elnashaie, S.S.E.H. *J. Power Sources* 195(17), 2010, 5749-5760.

16. Abashar, M.E.E. *Int. J. Hydrogen Energy* 38(2), 2013, 861-869.

17. Park, S.; Yoo, J.; Han, S.J.; Song, J.H.; Lee, E.J.; Song, I.K. *Int. J. Hydrogen Energy* 42(22), 2017, 15096-15106.

18. Bang, Y.; Han, S.J.; Seo, J.G.; Youn, M.H.; Song, J.H.; Song, I.K. *Int. J. Hydrogen Energy* 37(23), 2012, 17967-17977.

19. Wang, Y.; Sun, K.; Zhang, S.; Xu, L.; Hu, G.; Hu, X. *J. Energy Inst.* 98, 2021, 85-97.

20. Li, Y.; Zhang, L.; Zhang, Z.; Liu, Q.; Zhang, S.; Liu, Q.; Hu, G.; Wang, Y.; Hu, X. *Appl. Catal., A* 584, 2019, 117162.

21. Guo, Y.; Li, H.; Kameyama, H. *Chem. Eng. Sci.* 66(23), 2011, 6287-6296.

22. Chick, L.A.; Marina, O.A.; Coyle, C.A.; Thomsen, E.C. *J. Power Sources* 236, 2013, 341-349.

23. Belzunce, P.S.; Cadús, L.E.; Rodríguez, M.L. *Chem. Eng. Process.* 164, 2021, 108383.

24. Zanfir, M.; Gavriilidis, A. *Chem. Eng. Sci.* 56(8), 2001, 2671-2683.

25. Fukuhara, C.; Igarashi, A. *Chem. Eng. Sci.* 60(24), 2005, 6824-6834.

26. Kawamura, Y.; Ogura, N.; Yamamoto, T.; Igarashi, A. *Chem. Eng. Sci.* 61(4), 2006, 1092-1101.

27. Ioannides, T.; Verykios, X.E. *Catal. Today* 46(2-3), 1998, 71-81.

28. Piga, A.; Verykios, X.E. *Catal. Today* 60(1-2), 2000, 63-71.

29. Zanfir, M.; Gavriilidis, A. *Chem. Eng. Sci.* 57(9), 2002, 1653-1659.

30. Zanfir, M.; Gavriilidis, A. *Chem. Eng. J.* 86(3), 2002, 277-286.

31. Lakhete, P.; Janardhanan, V.M. *Chem. Eng. Sci.* 110, 2014, 13-19.

32. Janardhanan, V.M.; Appari, S.; Jayanti, S.; Deutschmann, O. *Chem. Eng. Sci.* 66(3), 2011, 490-498.

33. Brown, R.C. *Joule*, 4(11), 2020, 2268-2289.

34. Tonkovich, A.Y.; Perry, S.; Wang, Y.; Qiu, D.; LaPlante, T.; Rogers, W.A. *Chem. Eng. Sci.* 59(22-23), 2004, 4819-4824.

35. Roychowdhury, S.; Sundararajan, T.; Das, S.K. *Int. J. Heat Mass Transfer* 139, 2019, 660-674.

36. Tonkovich, A.L.Y.; Yang, B.; Perry, S.T.; Fitzgerald, S.P.; Wang, Y. *Catal. Today* 120(1), 2007, 21-29.

37. Tonkovich, A.; Kuhlmann, D.; Rogers, A.; McDaniel, J.; Fitzgerald, S.; Arora, R.; Yuschak, T. *Chem. Eng. Res. Des.* 83(6), 2005, 634-639.

38. Gavriilidis, A.; Angeli, P.; Cao, E.; Yeong, K.K.; Wan, Y.S.S. *Chem. Eng. Res. Des.* 80(1), 2002, 3-30.

39. Mettler, M.S.; Stefanidis, G.D.; Vlachos, D.G. *Chem. Eng. Sci.* 66(6), 2011, 1051-1059.

40. Cao, C.; Zhang, N.; Dang, D.; Cheng, Y. *Fuel Process. Technol.* 167, 2017, 78-91.

41. Lerou, J.J.; Tonkovich, A.L.; Silva, L.; Perry, S.; McDaniel, J. *Chem. Eng. Sci.* 65(1), 2010, 380-385.

DOI: http://dx.doi.org/10.32571/ijct.1060520 E-ISSN: 2602-277X

42. Murphy, D.M.; Manerbino, A.; Parker, M.; Blasi, J.; Kee, R.J.; Sullivan, N.P. *Int. J. Hydrogen Energy* 38(21), 2013, 8741-8750.

43. Baldea, M.; Daoutidis, P. *Chem. Eng. Sci.* 62(12), 2007, 3218-3230.

44. Zanfir, M.; Gavriilidis, A. *Chem. Eng. Res. Des.* 82(2), 2004, 252-258.

45. Kolios, G.; Frauhammer, J.; Eigenberger, G. *Chem. Eng. Sci.* 55(24), 2000, 5945-5967.

46. Tiemersma, T.P.; Kolkman, T.; Kuipers, J.A.M.; Annaland, M.V.S. *Chem. Eng. J.* 203, 2012, 223-230.

47. Herdem, M.S.; Mundhwa, M.; Farhad, S.; Hamdullahpur, F. *Energy Convers. Manage.* 180, 2019, 149-161.

48. Engelbrecht, N.; Everson, R.C.; Bessarabov, D.; Kolb, G. *Chem. Eng. Process.* 157, 2020, 108164.

49. Reitz, T.L.; Ahmed, S.; Krumpelt, M.; Kumar, R.; Kung, H.H. *J. Mol. Catal. A: Chem.* 162(1-2), 2000, 275-285.

50. Peppley, B.A.; Amphlett, J.C.; Kearns, L.M.; Mann, R.F. *Appl. Catal., A* 179(1-2), 1999, 31-49.

51. Park, G.G.; Seo, D.J.; Park, S.H.; Yoon, Y.G.; Kim, C.S.; Yoon, W.L. *Chem. Eng. J.* 101(1-3), 2004, 87-92.

52. Park, G.G.; Yim, S.D.; Yoon, Y.G.; Kim, C.S.; Seo, D.J.; Eguchi, K. *Catal. Today* 110(1-2), 2005, 108-113.

53. Chu, X.; Zeng, X.; Zheng, T.; Zhuang, W.; Yang, Y.; Zhou, W.; Hong, Y. *Int. J. Hydrogen Energy* 45(41), 2020, 20859-20874.

54. Lu, W.; Zhang, R.; Toan, S.; Xu, R.; Zhou, F.; Sun, Z.; Sun, Z. *Chem. Eng. J.* 429, 2022, 132286.

55. Stefanidis, G.D.; Vlachos, D.G.; Kaisare, N.S.; Maestri, M. *AIChE J.* 55(1), 2009, 180-191.

56. Stefanidis, G.D.; Vlachos, D.G. *Chem. Eng. Technol.* 31(8), 2008, 1201-1209.

57. Zanfir, M.; Gavriilidis, A. *Chem. Eng. Sci.* 58(17), 2003, 3947-3960.

58. Cao, C.; Dang, D.; Li, Y.; Xu, J.; Cheng, Y. *Chem. Eng. Process.* 132, 2018, 218-228.